

## Ellipsometric study of interband transitions in orthorhombic GeS

S. Logothetidis,\* L. Viña, and M. Cardona

*Max-Planck-Institut für Festkörperforschung, Heisenbergstrasse 1, D-7000 Stuttgart 80, Federal Republic of Germany*

(Received 1 October 1984)

Ellipsometric measurements have been used to determine the principal components of the dielectric tensor of orthorhombic crystalline GeS between 1.66 and 5.5 eV. Measurements have been taken from the cleavage plane and a second plane perpendicular to it. Calculations of the dielectric tensor have been done, using measurements at a large number of angles of incidence from the two surfaces. Critical-point energies for the light vector  $\mathbf{E}$  parallel to the  $\mathbf{a}, \mathbf{b}, \mathbf{c}$  directions and their broadening parameters were obtained by an analysis of the second-derivative spectra. The critical-point energies show only weak dependence on polarization.

### I. INTRODUCTION

The layerlike orthorhombic chalcogenides (GeS, GeSe, SnS, and SnSe) have recently attracted considerable interest.<sup>1-6</sup> Nevertheless, relatively little is known about these materials as compared with their cubic IV-VI compound counterparts (PbS, PbSe, and PbTe).

GeS is one of the few compound semiconductors which can be easily produced in both crystalline and amorphous forms<sup>7,8</sup> and, as concluded in Refs. 9 and 10, its structure is intermediate between layerlike and three dimensional. During the past years increasing interest has been devoted to the study of GeS: Infrared reflectivity and Raman scattering,<sup>9</sup> Raman measurements,<sup>11</sup> reflectivity for polarized light,<sup>1,12-14</sup> electron-energy-loss spectroscopy,<sup>1,15</sup> absorption,<sup>16-19</sup> photoconductivity<sup>16,17,20</sup> and electrical conductivity,<sup>20</sup> thermorefectance,<sup>21</sup> x-ray photoemission,<sup>22</sup> angle-resolved photoemission,<sup>10,22</sup> temperature dependence of fundamental-gap measurements,<sup>19</sup> and band-structure calculations<sup>10,22</sup> have been extensively carried out. The object of much of this work is to obtain information concerning the dielectric function and the band structure of GeS.

While the rhombohedral structure of the GeTe type arises from a distortion of the rocksalt structure, a quasi-tetragonal deformation leads to the structure of the GeS orthorhombic type.<sup>23</sup> The GeS structure, belonging to the orthorhombic space group  $D_{2h}^{16}$  ( $Pnma$ ) and nearly isomorphic to that of black phosphorus, cleaves in an exceptionally easy manner. It also exhibits considerable optical anisotropy, at least in the low-energy region.<sup>9,15</sup> Taking the  $c$  axis to be perpendicular to the cleavage plane and the other two ( $a$  and  $b$ ) lying in it, we expect different optical spectra for polarized light with electric vectors  $\mathbf{E}$  parallel to the  $\mathbf{a}, \mathbf{b}, \mathbf{c}$  directions, and especially for  $\mathbf{E}||\mathbf{c}$  where  $\mathbf{c}$  is a unit vector parallel to the  $c$  direction.<sup>24</sup> The primitive cell, with lattice constants  $a=4.30$  Å,  $b=3.64$  Å, and  $c=10.47$  Å,<sup>25</sup> contains eight atoms and covers two adjacent double layers. Within a layer, each atom has three nearest neighbors with bond distances 2.441 Å and two next-nearest neighbors at 3.27 Å. The sixth bond, between adjacent layers, has a length of 3.278 Å.

The layer structure and the optically biaxial nature of

orthorhombic GeS present some difficulties concerning measurements from cut and polished faces perpendicular to the cleavage plane. Hence, existing determinations of the optical constants for light polarized parallel to the  $c$  direction ( $\mathbf{E}||\mathbf{c}$ ) are not very reliable, as they were performed on such cut and polished samples which usually exhibit the grain of the perpendicular cleavage planes. Only reflectivity with polarized light,<sup>13</sup> photoconductivity, and electrical conductivity<sup>20</sup> measurements have been performed for surfaces perpendicular to the cleavage plane.

In the present paper we report the dielectric constants of GeS at room temperature for all three principal polarizations as determined with spectral ellipsometry in the photon-energy range from 1.66 to 5.5 eV. Measurements were performed on single crystals for two faces of these crystals, one parallel to the cleavage plane and another perpendicular to this plane. We were able to test the approximate ellipsometric method proposed by Aspnes for biaxial crystals<sup>26</sup> and to compare with the dielectric constants calculated with an iterative scheme based on several angles of incidence. A line-shape analysis of the numerically obtained second-derivative spectra of the principal components of the complex dielectric tensor [ $\epsilon_j = (\epsilon_1)_j + i(\epsilon_2)_j$ ,  $j = a, b, c$ ] near the critical points (CP's) allowed us to obtain critical energies ( $E$ ), broadening parameters ( $\Gamma$ ), and strengths ( $A$ ). Most of the observed structures can be assigned to specific transitions by comparison with band-structure calculations.<sup>22</sup>

In the following section a description of the method is first given. The experimental details are described in Sec. III, the results are presented in Sec. IV and discussed in Sec. V.

### II. OPTICAL ANALYSIS

The  $4 \times 4$  matrix method<sup>27-30</sup> offers a general unified approach for the determination of all the optical parameters in any anisotropic material. Unfortunately, due to its complexity, this method has been only applied in a few cases.<sup>29</sup> The explicit expressions for the reflection coefficients in anisotropic materials have been derived for a few of them with special symmetry.<sup>31</sup> In a recent paper

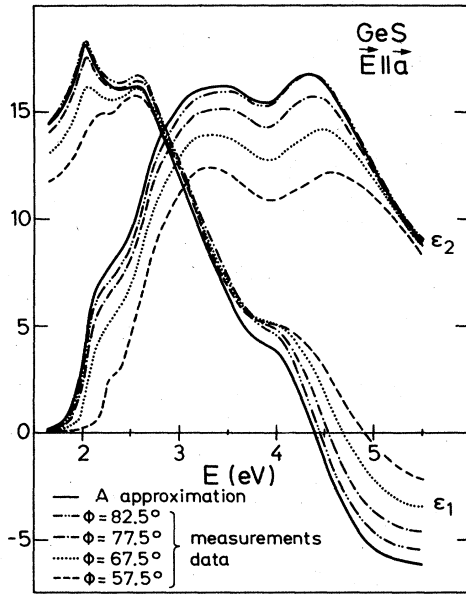


FIG. 1. Real and imaginary parts of the pseudodielectric function from measurements with the ac plane of incidence perpendicular to the cleavage plane of GeS at different angles of incidence:  $\cdots$ ,  $\phi = 82.5^\circ$ ;  $\cdots\cdots$ ,  $\phi = 77.5^\circ$ ;  $\cdots\cdots\cdots$ ,  $\phi = 67.5^\circ$ ;  $\cdots\cdots\cdots$ ,  $\phi = 57.5^\circ$ . The solid line corresponds to the  $\epsilon_a$  pseudodielectric function as calculated with the approximate technique of Eq. (3), approximation A.

Aspnes<sup>26</sup> has developed an approximate solution of the ellipsometric equations which can be used to calculate the principal components of the dielectric tensor in biaxial materials. The method assumes that the principal components of the dielectric tensor  $\epsilon_a$ ,  $\epsilon_b$ , and  $\epsilon_c$  can be obtained by applying small corrections to an isotropic mean value  $\epsilon$ ,

$$\epsilon_j = \epsilon + \Delta\epsilon_j, \quad j = a, b, c \quad (1)$$

and that the perturbation  $\Delta\epsilon_j$  can be treated to first order.

For an orthorhombic material oriented so that one of the principal axes (e.g.,  $c$ ) is perpendicular to the surface, we choose the plane of incidence to contain another principal axis ( $a$ ), and thus to be normal to the third one ( $b$ ). In this case the reflection matrix is diagonal<sup>31</sup> and the reflection coefficients for  $s$ - and  $p$ -polarized light are given by the equations<sup>32</sup>

$$r_p^{ik} = \frac{\epsilon_i^{1/2} \cos\phi_1 - \epsilon_0^{1/2} \left[ 1 - \frac{\sin^2\phi}{\epsilon_k} \right]^{1/2}}{\epsilon_i^{1/2} \cos\phi_1 + \epsilon_0^{1/2} \left[ 1 - \frac{\sin^2\phi}{\epsilon_k} \right]^{1/2}}, \quad (2a)$$

$$r_s^{ik} = \frac{\epsilon_0^{1/2} \cos\phi_1 - (\epsilon_j - \sin^2\phi)^{1/2}}{\epsilon_0^{1/2} \cos\phi_1 + (\epsilon_j - \sin^2\phi)^{1/2}}, \quad (2b)$$

where

$$\cos\phi_1 = (1 - \sin^2\phi/\epsilon_0)^{1/2}.$$

$\phi$  represents the angle of incidence,  $\epsilon_0$  the dielectric con-

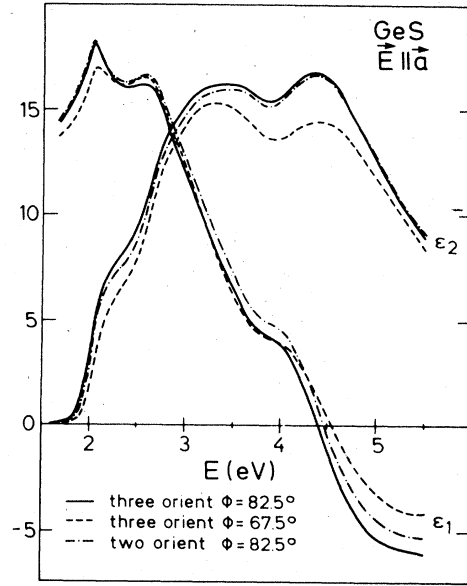


FIG. 2. Real and imaginary parts of the pseudodielectric function  $\epsilon_a$  of GeS as obtained by the approximate technique using three orientations:  $\cdots$ , approximation A;  $\cdots\cdots$ , from the cleavage plane only, with angles of incidence  $\phi = 67.5^\circ$ ;  $\cdots\cdots\cdots$ , from the cleavage plane only, with angles of incidence  $\phi = 82.5^\circ$ .

stant of a possible overlayer (if there is no overlayer  $\epsilon_0 = 1$ ),  $\epsilon_m$  ( $m = i, j, k$ ) are the principal components of the dielectric tensor, and  $i, k$  the principal axes contained in the  $ik$  plane of incidence.

Ellipsometry measures the relative complex reflection ratio  $\rho_{ik} = r_p^{ik}/r_s^{ik}$ , from which one can calculate the pseudodielectric constant  $\epsilon_{ik}$  using the two-phase model (ambient medium) under the assumption of an isotropic medium.<sup>31</sup> According to Aspnes<sup>26</sup> we may derive the  $\epsilon_m$  ( $m = a, b, c$ ) pseudodielectric constants with the aid of Eq. (1) from the solution of the simultaneous linear equations:

$$\frac{\epsilon - \sin^2\phi}{\epsilon - 1} \Delta\epsilon_i - \frac{\epsilon \cos^2\phi - \sin^2\phi}{\epsilon - 1} \Delta\epsilon_j - \frac{1}{\epsilon - 1} \Delta\epsilon_k = (\epsilon_{ik} - \epsilon) \sin^2\phi. \quad (3)$$

$ik = (ac, bc, ca)$  or another selection of pairs of principal axes defining three planes of incidence. The mean value  $\epsilon$  is calculated from the experimental  $\epsilon_{ik}$  ( $ac, bc, ca$ ) in the effective-medium approximation<sup>33,34</sup> with equal admixtures of the three components ( $x_{ac} = x_{bc} = x_{ca}$ ):<sup>26</sup>

$$x_{ac} \frac{\epsilon_{ac} - \epsilon}{\epsilon_{ac} + 2\epsilon} + x_{bc} \frac{\epsilon_{bc} - \epsilon}{\epsilon_{bc} + 2\epsilon} + x_{ca} \frac{\epsilon_{ca} - \epsilon}{\epsilon_{ca} + 2\epsilon} = 0. \quad (4)$$

On the other hand, ellipsometric measurements of the complex relative reflection ratio  $\rho_{ik}$  at an adequate number of properly chosen angles of incidence provide enough information to determine, without making the linear approximation of Eq. (1), the principal dielectric tensor components. Two iterative methods can be used to determine the dielectric constants of a crystal with orthorhombic symmetry. In one of these, where the measurements

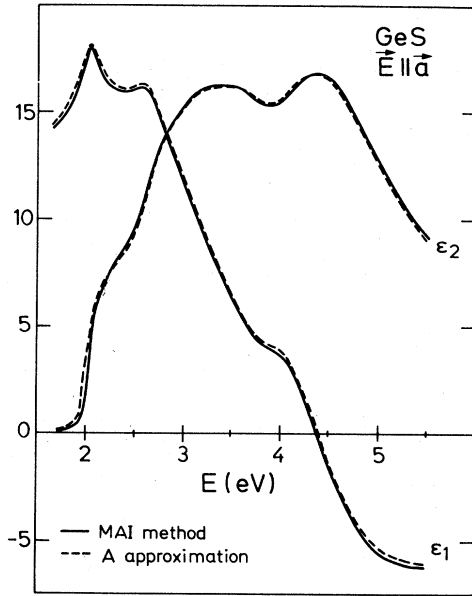


FIG. 3. Real and imaginary parts of the dielectric function  $\epsilon_a$  of GeS as obtained with the MAI method (solid lines) and the pseudodielectric function  $\epsilon_a$  (dashed lines) calculated with approximation A.

may be taken only from a single-crystal surface<sup>35,36</sup> in order to overcome the difficulties due to the weak dependence of the complex reflection ratio  $\rho_{ik}$  on the  $\epsilon_k$  dielectric constant, we have to use an efficient and suitable fitting algorithm.<sup>36</sup> The second method requires measurements from two different surfaces of the crystal.<sup>35,37</sup> In the case of layer materials, the first method offers the advantage that measurements may be taken from a freshly cleaved plane. However, obtaining acceptable solutions requires the measurement of ellipsometric quantities to be as free as possible from random and systematic errors. The second kind of measurement, for different orientations and multiple angles of incidence (MAI) in each orientation, provides in principle enough information to determine not only the principal dielectric tensor components, but also the optical parameters of an unknown overlayer on a surface (i.e., the cut and polished surface perpendicular to the cleavage plane in layer-type orthorhombic materials). In this case for a certain photon energy  $\omega$  we can derive the following nonlinear relations that relate the measured ellipsometric quantities  $\rho_{ik}^m$  to the optical parameters:

$$\text{Re}(\rho_{ik}^m) = X_{ik}^{\text{calc}}(\epsilon_a, \epsilon_b, \epsilon_c, \epsilon_0, d, \phi_n),$$

$$\text{Im}(\rho_{ik}^m) = Y_{ik}^{\text{calc}}(\epsilon_a, \epsilon_b, \epsilon_c, \epsilon_0, d, \phi_n),$$

$$ik = (ac, bc, ba, ca) \quad (5)$$

where  $n$  labels the different angles of incidence in the  $ik$  plane of incidence (or orientation),  $\epsilon_0 (= \epsilon_{10} + i\epsilon_{20})$ , and  $d$  is the overlayer's dielectric constant and thickness if it is present on the  $bc$  surface. The superscript calc means calculated.

In the case of a three-phase (ambient-overlayer-substrate) system the total reflection coefficients for the  $s$

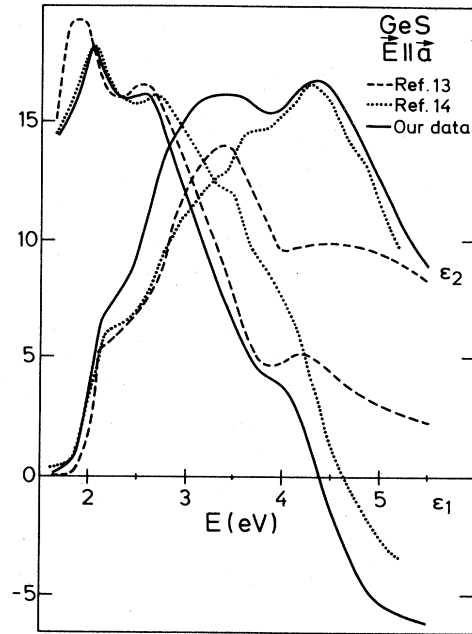


FIG. 4. Solid lines, real and imaginary parts of the dielectric function  $\epsilon_a$  of GeS obtained by us at room temperature. Dashed lines, corresponding results reported in Ref. 13. Dotted lines, results reported in Ref. 14.

and  $p$  components of light are given by the equations<sup>31</sup>

$$R_m^{ij} = \frac{r_{0m} - r_m^{ij} e^{i2\beta}}{1 + r_{0m} r_m^{ij} e^{i2\beta}},$$

$$m = p \text{ or } s \text{ and } ij = (ba, ca) \quad (6)$$

and

$$r_{0s} = \frac{\cos\phi - (\epsilon_0 - \sin^2\phi)^{1/2}}{\cos\phi + (\epsilon_0 - \sin^2\phi)^{1/2}}, \quad (7a)$$

$$r_{0p} = \frac{\epsilon_0^{1/2} \cos\phi - (\epsilon_0 - \sin^2\phi)^{1/2}}{\epsilon_0^{1/2} \cos\phi + (\epsilon_0 - \sin^2\phi)^{1/2}}, \quad (7b)$$

where

$$\beta = \frac{2\pi d}{\lambda} (\epsilon_0 - \sin^2\phi)^{1/2}$$

is the phase angle, and  $r_m^{ij}$  is given by Eq. (2).

The computational problem consists of searching for a vector  $A = (\epsilon_a, \epsilon_b, \epsilon_c, \epsilon_0, d)$  for which the error function

$$G(A) = \sum_{ik} \sum_{j=1}^n \{ [X_{ik}^m - X_{ik}^c(A, \phi_j)]^2 + [Y_{ik}^m - Y_{ik}^c(A, \phi_j)]^2 \} \quad (8)$$

is minimized. Equation (8) can be generalized to include several angles  $\phi$  for a given plane of incidence. For measurements on cleaved surfaces we assume that these surfaces are free from overlayers. The convergence problem in this case is easier than that of measurements only from

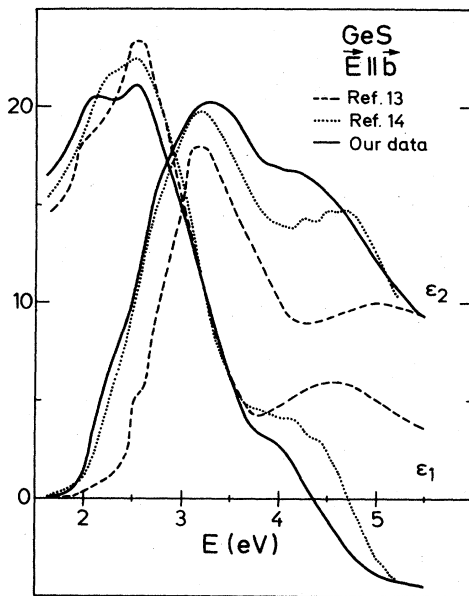


FIG. 5. Real and imaginary parts of the dielectric function  $\epsilon_b$  of GeS. The symbols are the same as in Fig. 4.

the cleavage plane,<sup>35,36</sup> because the error function  $G(A)$  depends strongly on all the parameters. On the other hand, it is more complicated due to the large number of measurements from different orientations (or planes of incidence) that are required, especially if we have to consider a three-phase system for one of the surfaces.

### III. EXPERIMENTAL

The measurements were taken on single undoped crystal of GeS grown by vacuum sublimation.<sup>38</sup> The overall size of the ingots was  $\sim 1.8$  cm diameter and  $\sim 4$  cm total length. Thus it was possible to obtain single-crystal samples with usable cleaved surfaces of more than  $2$  cm<sup>2</sup>. Measurements on the cleavage plane were performed on freshly cleaved surfaces peeled off with adhesive tape immediately before the measurements. The surfaces of the cleavage plane were mirrorlike with no visible steps or imperfections. The  $a$ ,  $b$ , and  $c$  axes were located on the appropriate surfaces using standard Laue x-ray pictures. Samples for measurements on planes perpendicular to the  $a$  and  $b$  axes are considerably more difficult to prepare since they require cutting perpendicular to the cleavage plane and a polishing procedure. We used planes prepared in such way, parallel to the  $b$  axis and perpendicular to the cleavage plane. For this purpose the samples were sawed with a diamond-impregnated wire. The surfaces to be measured were very gently and carefully mechanically lapped and polished with  $\text{Al}_2\text{O}_3$  powder followed by an etch polish with Syton (Syton W30, Brenntag AG, 4330 Mülheim/Ruhr 12, Federal Republic of Germany). Finally, these surfaces were polished with a bromine-methanol solution.<sup>39</sup> The specimen for ellipsometric measurements perpendicular to the cleavage plane was chosen from a series of available large crystals

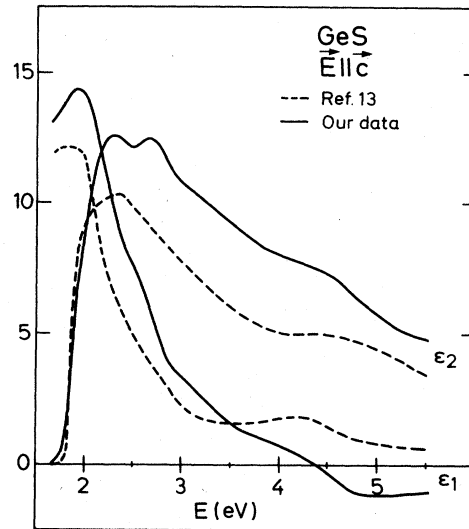


FIG. 6. Solid lines, real and imaginary parts of the dielectric function  $\epsilon_c$  of GeS at room temperature. Dashed lines, corresponding results reported in Ref. 14.

which were prepared without showing any cleavage lines in a region  $2 \times 0.30$  cm<sup>2</sup> of its polished surface. For Fresnel equations (2) to hold two of the principal axes must lay on the plane of incidence and hence the third be perpendicular to it.<sup>31</sup> Therefore great care was needed in orienting the sample parallel to the  $a$ ,  $b$ , and  $c$  axes. For this reason special attention was paid to the adjustment of our samples with the aid of an extra goniometric table in our ellipsometer sample holder. In this way the error in the orientation of the crystallographic axes was less than  $2^\circ$  in all the cases. During the measurements the samples were kept at room temperature in a windowless cell in flowing dry  $\text{N}_2$  to minimize possible surface contamination effects.<sup>14</sup> Measurements performed with a rotating-analyzer ellipsometer<sup>40</sup> are described in detail elsewhere.<sup>41</sup>

### IV. RESULTS

The real and imaginary parts of the pseudodielectric functions  $\epsilon_{ik}$  for four orientations with several angles of incidence for each orientation were calculated from the complex reflectance ratios by using the two-phase model. The spectra of the pseudodielectric function  $\epsilon_{ac}$  for four selected angles of incidence are shown in Fig. 1 and compared with the pseudodielectric function  $\epsilon_a$  calculated with the aid of Eqs. (3) and angles of incidence for three different orientations  $ac$ ,  $bc$ , and  $ca$ ,  $\phi = 82.5^\circ$ ,  $82.5^\circ$ , and  $72.5^\circ$ , respectively (this approximation is hereafter called approximation A). In Fig. 1 we can see that the contribution of the  $\epsilon_b$  component of the dielectric tensor to the  $\epsilon_{ac}$  pseudodielectric constant decrease as the angle of incidence increases, and for an angle of incidence  $\phi = 82.5^\circ$ , the  $\epsilon_{ac}$  spectra nearly coincide with  $\epsilon_a$ . Figure 2 shows the results for three cases: the solid line represents approximation A with  $\phi = 82.5^\circ$ , the dashed line represents

TABLE I. Effective number of electrons per atom  $n_{\text{eff}}(\omega_M)$  and static dielectric constant  $\epsilon_{0,\text{eff}}(\omega_M)$  as given by sum rules, Eq. (8).

	E  a	E  b	E  c
$n_{\text{eff}}$	1.32 <sup>a</sup>	1.46 <sup>a</sup>	
	1.18 <sup>b</sup>	1.21 <sup>b</sup>	0.71 <sup>b</sup>
	5.98 <sup>c</sup>	6.39 <sup>c</sup>	3.06 <sup>c</sup>
	1.63 <sup>d</sup>	1.79 <sup>d</sup>	1.01 <sup>d</sup>
$\epsilon_{0,\text{eff}}$	7.92 <sup>a</sup>	8.89 <sup>a</sup>	
	7.15 <sup>b</sup>	6.91 <sup>b</sup>	5.89 <sup>b</sup>
	10.33 <sup>c</sup>	10.48 <sup>c</sup>	7.15 <sup>c</sup>
	9.49 <sup>d</sup>	10.01 <sup>d</sup>	7.91 <sup>d</sup>
	11.1 <sup>e</sup>	12.2 <sup>e</sup>	8.4 <sup>e</sup>

<sup>a</sup>Reference 14;  $\omega_M=5.2$  eV.

<sup>b</sup>Reference 13;  $\omega_M=5.5$  eV

<sup>c</sup>Reference 13;  $\omega_M=25$  eV.

<sup>d</sup>Our data;  $\omega_M=5.5$  eV.

<sup>e</sup>From Ref. 12 and our measurements extrapolated to  $\omega=0$ .

the same approximation with  $\phi=67.5^\circ$  for all three orientations, and the dashed-dotted line represents the  $\epsilon_a$  spectrum estimated with the aid of Eqs. (3), without taking into account the  $\epsilon_c$  component ( $\Delta\epsilon_c=0$ ) (two orientations) for angles of incidence  $\phi=82.5^\circ$ . From the comparison it becomes clear that the  $\epsilon_c$  component is not so important for ellipsometric measurements obtained with the  $a$  and  $c$  ( $ac$ ) or with the  $b$  and  $c$  ( $bc$ ) axes lying in the plane of incidence, as already pointed out by Aspnes.<sup>28</sup>

In Fig. 3 a comparison is made between the spectra of the A approximation and the spectra of  $\epsilon_a$  calculated by the MAI method from the measurements that have been done with the  $ac$ ,  $bc$ ,  $ba$ , and  $ca$  axes in the plane of incidence, respectively. We have used three angles of incidence for each orientation. As we can see the agreement between these two spectra is excellent. Thus we conclude that the approximate method A as suggested by Aspnes<sup>26,42</sup> gives good results for the estimation of the dielectric tensor components even in the case that measurements are impossible for one orientation. However, in order to get accurate absolute values, measurements have to be carried out at large angles of incidence.

Figures 4–6 show our spectra of the dielectric function of GeS for the three principal polarizations as obtained by MAI method (solid lines) in comparison with data of Ref. 13 (dashed lines) and Ref. 14 (dotted lines). They agree reasonably well with those of Ref. 14 for polarizations E||a and E||b, but disagree considerably with reflectivity data of Ref. 13, especially for energies higher than 3.5 eV, a fact that was also mentioned in Ref. 1. The main feature in these spectra is the presence of comparatively broad peaks. This may result from the possible overlap of closely spaced critical points in this layer-type compound of relatively low symmetry.

In order to check the consistency of the obtained spectra and to compare with already reported results we have evaluated the well-known sum rules for the oscillator strengths:<sup>43</sup>

$$[n_{\text{eff}}(\omega_M)]_j = \frac{m}{2\pi^2 e^2 N} \int_0^{\omega_M} \omega [\epsilon_2(\omega)]_j d\omega, \quad (9a)$$

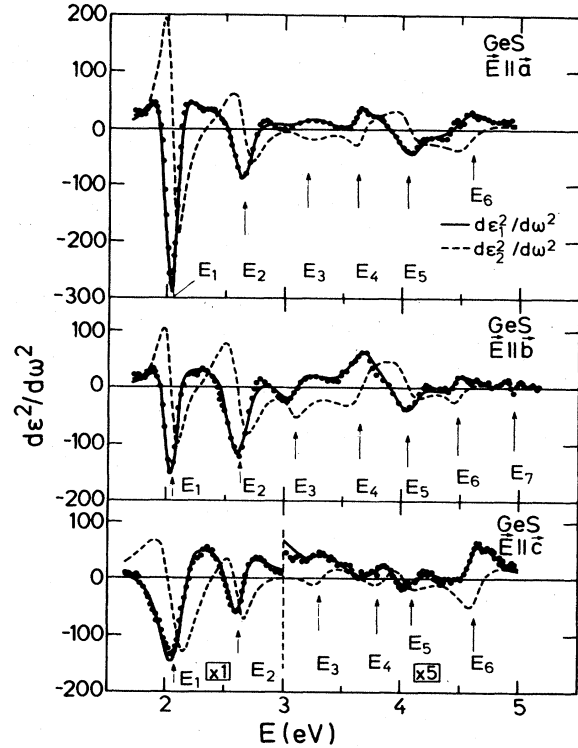


FIG. 7. Second derivatives of the real (solid line) and imaginary (dashed line) parts of the dielectric function of GeS as a function of photon energy for the three principal polarizations obtained from a critical-point fit. The experimental data are only given for  $d^2\epsilon_1/d\omega^2$ . The vertical scale for E||c at the energy region 3 to 5 eV has been expanded by a factor of 5.

$$[\epsilon_{0,\text{eff}}(\omega_M)]_j = 1 + \frac{2}{\pi} \int_0^{\omega_M} \frac{[\epsilon_2(\omega)]_j}{\omega} d\omega, \quad j=(a,b,c) \quad (9b)$$

where  $n_{\text{eff}}(\omega_M)$  is the number of electrons per atom contributing to the optical properties in the range  $\omega_M$  and  $m$  and  $e$  are the mass and charge of free electrons, respectively. The  $n_{\text{eff}}$  values calculated from our data with the upper limit  $\omega_M=5.5$  eV for E||a and E||b are comparable with the corresponding values from the data of Ref. 14 (see Table I), but are larger than those of Ref. 13 for all polarizations. Our values of  $n_{\text{eff}}$  for E||a and E||b, and those of Ref. 14 for  $\omega_M=5.5$  eV, lie around 1.7/atom, only slightly lower than that for cubic SnTe (2/atom).<sup>44</sup>  $n_{\text{eff}}$  for GeS at  $\omega=5.5$  eV would be expected to be lower than the value for SnTe for two reasons: (1) The average valence-conduction band separations for GeS are larger than those of SnTe. (2) The  $d$ -valence electrons give a contribution to  $n_{\text{eff}}$  in the case of Te, Ge, and Sn, but S has no filled  $d$  states. Thus we believe the value of  $n_{\text{eff}} \approx 1.7/\text{atom}$  for  $\omega_M=5.5$  eV to be reasonable and the value found from the data of Ref. 13 (1.2/atom) to be too low. However, the  $n_{\text{eff}}$  from Ref. 13 for  $\omega_M=25$  eV for E||a and E||b ( $n_{\text{eff}} \approx 6/\text{atom}$ ) seems to be reasonable, rather too high than too low when compared with the cor-

TABLE II. Critical-point energies of interband transitions in GeS for all three polarizations. Values correspond to room temperature (all energies in eV).

	Our data	Reference 13, reflectivity peaks	Reference 14	Reference 1, reflectivity peaks	Theoretical Reference 22
<b>E  a polarization</b>					
$E_0$			1.588	~1.65	1.2
$E_1$	2.037(10)	2.0	2.034	~2.2	2.2–2.4
$E_2$	2.637(6)	2.8	2.642		2.5–2.7
$E_3$	3.162(46)				
$E_4$	3.628(17)	3.4	3.55	3.5	3.2–3.6
$E_5$	4.031(13)		4.10	4.3	~4.2
$E_6$	4.53(9)	4.9	4.3		~4.4
					~5.0
<b>E  b polarization</b>					
$E_0$			1.661		1.2
$E_1$	2.047(6)	2.1	2.15	~2.2	1.8
$E_2$	2.610(9)	2.7	2.52		~2.6
			2.63		~3.0
$E_3$	3.096(17)		2.98		~3.1
			3.28		~3.4
$E_4$	3.668(19)		3.45	3.3	~3.8
$E_5$	4.043(12)		4.15		~4.0
$E_6$	4.563(28)	5.0	4.50	4.5	~4.5
$E_7$	~4.95		4.9		~5.0
<b>E  c polarization</b>					
$E_0$				~1.65	
$E_1$	2.078(18)	2.2			
$E_2$	2.623(17)	2.5			
$E_3$	3.310(45)	3.3			
$E_4$	3.788(85)				
$E_5$	4.028(25)				
$E_6$	4.623(41)	4.7			

responding data for SnTe ( $n_{\text{eff}} \approx 5/\text{atom}$ ). The values of  $n_{\text{eff}}$  for  $\mathbf{E}||\mathbf{c}$  are, in all cases, much smaller than the corresponding values for  $\mathbf{E}||\mathbf{a}$  and  $\mathbf{E}||\mathbf{b}$ . One may be tempted to attribute the difference to the poor quality of the polished surface which weighs significantly in the data for  $\mathbf{E}||\mathbf{c}$ . Nevertheless, the fact that all measurements yield low values for  $n_{\text{eff}}$  with  $\mathbf{E}||\mathbf{c}$  suggests that this may indeed be a consequence of the weak interlayer bonding. Similar effects are observed for other materials with the same structure such as GeSe (Ref. 5) and black P.<sup>45</sup>

The values of  $\epsilon_{0,\text{eff}}(\omega_M)$  obtained with Eq. (9b) are much closer to the experimental  $\epsilon_0$  than in the case of  $n_{\text{eff}}$  due to the faster convergence of the integral of Eq. (9b). Also for  $\epsilon_{0,\text{eff}}$  with  $\omega_M = 5.5$  eV we find that the data of Ref. 13 yield lower values than our data. It has been shown<sup>46</sup> that surface oxide layers and other defects lead, in general, to decrease of  $n_{\text{eff}}$  and  $\epsilon_{0,\text{eff}}$ . Hence we conclude that our data are better than those of Ref. 13. In any case the values of  $\epsilon_{0,\text{eff}}$  for  $\mathbf{E}||\mathbf{c}$  are also consistently smaller than the corresponding values for  $\mathbf{E}||\mathbf{a}$  and  $\mathbf{E}||\mathbf{b}$ , a fact which also holds for other similar layer materi-

als.<sup>5,45,47</sup> We believe that this may also be a consequence of the weak interlayer bonding. We note, however, that while for  $\mathbf{E}||\mathbf{a}$  and  $\mathbf{E}||\mathbf{b}$  our  $\epsilon_{0,\text{eff}}$  ( $\omega_M = 5.5$  eV) is about 2 units less than  $\epsilon_0$ , this difference is only  $\sim 0.5$  for  $\mathbf{E}||\mathbf{c}$ . This is somewhat surprising and may point out to errors in the  $\mathbf{E}||\mathbf{c}$  measurements which are heavily weighted by data for the polished surface.

In order to enhance structure present in the spectra and to obtain the  $cp$  parameters, we have numerically evaluated the derivative spectra of the complex dielectric function  $\epsilon_j$  ( $j = a, b, c$ ), computed by the MAI method from our ellipsometric data. In Fig. 7 we display the second-derivative spectra computed from the real part of the complex dielectric function for the three polarizations, together with the best fits to the second-derivative  $cp$  line shapes of the real and imaginary part of  $\epsilon_j$  ( $j = a, b, c$ ). Experimental points are only given for  $d^2\epsilon_1/d\omega^2$ . We assumed for the fitting of derivative spectra mixtures<sup>48,49</sup> of two-dimensional (2D) or three-dimensional (3D) critical points, which can be represented by<sup>49,50</sup>

$$\epsilon \sim c - A \ln(E - \omega - i\Gamma) e^{i\Phi} \quad \text{where } \Phi = 0 \text{ for minimum or } \Phi = \pi/2 \text{ for saddle point,} \quad (10a)$$

$$\epsilon \sim c - A(\omega - E + i\Gamma)^{1/2} e^{i\Phi} \quad \text{where } \Phi = 0 \text{ for } M_1 \text{ or } \Phi = \pi/2 \text{ for } M_2, \quad (10b)$$

TABLE III. Lorentzian broadening parameters of interband transitions, strengths, phase angles, and type of CP's in GeS.

	$\Gamma$ (meV)	Strength $A$	Phase angle $\Phi$ (deg)	Type of CP	Type of CP (Ref. 14)
<b>E  a polarization</b>					
$E_1$	98(10)	2.9(2)	5(2)	2d minimum and saddle	$M_0(M_1)$
$E_2$	150(13)	2.1(2)		2d minimum	$M_0(M_1)$
$E_3$	217(46)	6(1)	75(5)	$M_1$ and $M_2$	
$E_4$	105(17)	3.3(5)	85(6)	$M_1$ and $M_2$	$M_1(M_0)$
$E_5$	151(18)	6(1)	26(4)	$M_0$ and $M_1$	$M_1$
$E_6$	226(88)	8(3)		$M_1$	$M_2(M_1)$
<b>E  b polarization</b>					
$E_1$	99(12)	1.6(2)		2d minimum	$M_0$
$E_2$	162(19)	3.2(3)		2d minimum	$M_1(M_0)$
$E_3$	129(27)	5.1(7)	21(3)	$M_1$ and $M_2$	$M_1$
$E_4$	172(19)	12(2)	47(5)	$M_1$ and $M_2$	$M_1(M_2)$
	173(26)	1.3(4)		2d minimum	
$E_5$	187(26)	1.4(4)	34(5)	2d minimum and saddle	$M_1$
$E_6$	110(28)	2.6(6)	44(4)	$M_1$ and $M_2$	$M_1$
<b>E  c polarization</b>					
$E_1$	205(18)	6.4(6)	35(3)	2d minimum and saddle	
$E_2$	124(17)	1.4(2)	24(3)	2d minimum and saddle	
$E_3$	134(45)	0.6(2)		$M_2$	
$E_4$	139(85)	1.4(5)	39(6)	$M_1$ and $M_2$	
$E_5$	177(25)	0.2(1)		2d minimum	
$E_6$	153(41)	3.2(9)	81(7)	$M_1$ and $M_2$	

for 2D and 3D, respectively, where  $E$  means the CP energy and  $\Gamma$  the broadening parameter and  $A$  is a measure of the strength of the critical point.

In Fig. 7 we use the same labels for structures corresponding to CP's closely lying in energy for the three polarizations. The  $E_1$  CP for  $\mathbf{E}||\mathbf{a}$  gives a second derivative at least twice as large as in the case of the other two polarizations. We have found that the best representation for the  $E_1$  and  $E_2$  structures for all three polarizations is a 2D critical point (see Tables II and III). In the case of  $E_3$ ,  $E_4$ , and  $E_6$  structures, we have used a 3D  $M_1$  and  $M_2$  mixture for all three polarizations. A different relative contribution of  $M_1$  and  $M_2$  types corresponds to each of these three structures. Concerning the  $E_5$  structure, for  $\mathbf{E}||\mathbf{a}$  fitting can be done with a 3D  $M_0$  and  $M_1$  admixture. In the cases  $\mathbf{E}||\mathbf{b}$ ,  $\mathbf{E}||\mathbf{c}$ , this can be achieved either using a 2D minimum or a 2D mixture, although the former seems to give as good a representation as the latter. Lukeš *et al.*<sup>14</sup> have made a crude estimate of the type of CP's based on the characteristic shape of the  $(\epsilon_1)_j$  and  $(\epsilon_2)_j$  ( $j = a, b$ ) spectra. This kind of assignment causes difficulties, especially in CP's where two possible 3D structures overlap to give a line shape similar to a 2D CP,<sup>41</sup> a feature rather common in the measurements for GeS. On the other hand, spectroscopic ellipsometry yields directly the two components of the dielectric function and its derivatives. Hence it should be a more reliable technique to analyze the type of CP's.

## V. DISCUSSION

The difference in the relative strength of the  $\epsilon_2$  structures and the CP energies for the three polarizations may

sometimes be explained by different selection rules. The imaginary part of the dielectric function is given by<sup>51</sup>

$$[\epsilon_2(\omega)]_j = \frac{4\hbar^2 e^2}{\pi m^2 \omega^2} \int_{\text{BZ}} |M_{cv}^j|^2 \delta(E_c - E_v - \hbar\omega) dk, \quad j = a, b, c. \quad (11)$$

The transition strengths  $A$  are related to the square of the momentum matrix elements. These can be calculated from the pseudopotential wave functions but, unfortunately, this was not done in the few existing works on the band structure of GeS. Nevertheless, from the known symmetry properties of the wave functions, it is possible to find the appropriate selection rules. If the coordinates corresponding to the  $\mathbf{a}, \mathbf{b}, \mathbf{c}$  directions belong to different irreducible representations, we obtain different selection rules. In Ref. 5 the selection rules for the orthorhombic IV-VI compounds are given; they agree with those listed by Lukeš *et al.* for GeS (apparent discrepancies are only due to the notation<sup>14</sup>).

The crystal structure of GeS is nearly the same as that of black P except for the fact that in the latter all atoms are equal.<sup>28</sup> Both crystals have almost equal lattice parameters, they are isoelectronic, and the structure of the single puckered layers and the interlayer spacings are also similar. Hence, due to these similarities, a close relationship between their electronic properties is expected. This fact enables us to attempt a comparison with calculations for black P. The tight-binding approximation<sup>52</sup> and the self-consistent pseudopotential<sup>53</sup> techniques have been applied to calculate the band structure of black P and to interpret its optical and electrical properties. As mentioned in the preceding section the energy dependence of the

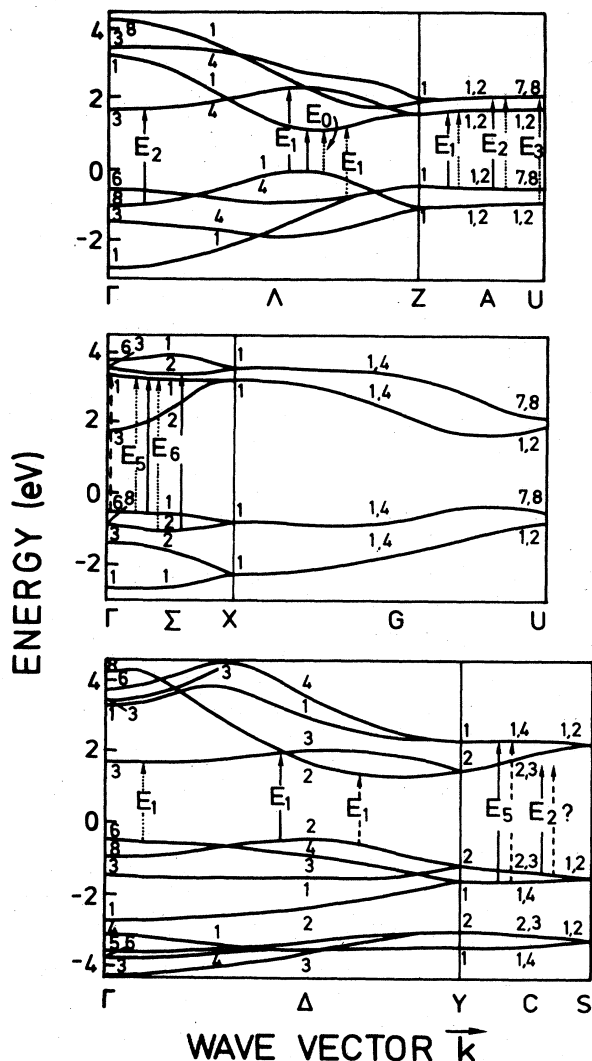


FIG. 8. Band structure of GeS in different directions in the BZ reproduced from Ref. 22. Dotted arrows indicate interband transitions allowed for  $E||a$ , dashed arrows the same for  $E||b$ , and solid arrows for  $E||c$ .

dielectric function for the three principal polarizations has been obtained for black P by means of self-consistent pseudopotential calculations.<sup>53</sup> In Ref. 45,  $[\epsilon_2(\omega)]_j$  was calculated with Eq. (11) and the corresponding  $[\epsilon_1(\omega)]_j$  were evaluated from  $[\epsilon_2(\omega)]_j$  by Kramers-Kronig transformation. There are some remarkable differences in the  $[\epsilon_2(\omega)]_j$  and  $[\epsilon_1(\omega)]_j$  calculated for the three directions: The oscillator strengths are distributed in different regions due to the fact that dipole transitions are sometimes allowed for one polarization and forbidden for the others. The polarization dependence of  $[\epsilon_1(\omega)]_j$  disappears for energies larger than 10 eV but the static dielectric constant is found to be strongly anisotropic. We can see in our results for GeS, and for larger or smaller energies in Refs. 1, 9, and 13, features similar to those mentioned above for black phosphorus. The two main peaks shown for  $\epsilon_2$  ( $E||a$ ) in Fig. 4 are also seen in the calcula-

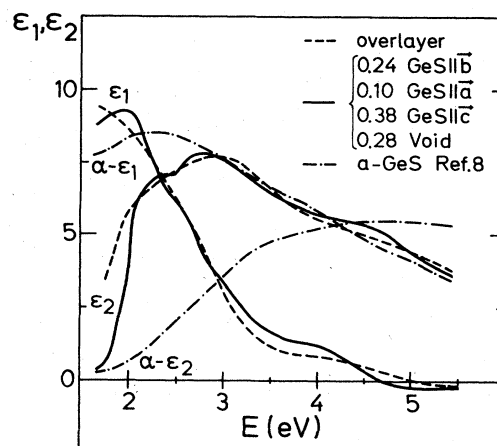


FIG. 9. Analysis of data with the MAI method under the assumption of the existence of an isotropic layer (thickness  $50 \pm 5$  Å). Dashed line, dielectric functions of the overlayer. The solid line shows an attempt to describe this overlayer as a composite medium of all principal components plus voids with relative compositions  $x$  given in the figure. The dashed-dotted line shows, for comparison, the dielectric constant of  $\alpha$ -GeS.

tions for black P [Fig. 4(b) of Ref. 45], slightly shifted to higher energies. Similar correspondence is found for  $E||b$ . We are, however, unable to see such correspondence for  $E||c$ .

Since our spectral region only covers the energy range from 1.66 to 5.5 eV, we were able to observe transitions derived only from the highest four valence and the lowest four conduction subbands.<sup>11,22</sup> In Ref. 54, using the linear combination of atomic orbitals approach and taking into account  $sp$  hybridization, it was concluded for the IV-VI compounds that the lower group of peaks in the reflectivity spectra<sup>55</sup> corresponds to electronic transitions from the anion to the cation, and not to  $p$ -bonding- $p$ -antibonding transitions.<sup>10,14,22,54</sup> This fact would reflect the ionic nature of these materials as discussed in Ref. 56. In Ref. 54, however, it is suggested that the highest reflectivity peaks are due to  $p$ -bonding- $p$ -antibonding combinations. Nevertheless, more precise calculations are necessary to provide a better understanding of the nature of the bonding in the IV-VI compounds.<sup>57</sup>

As seen in Fig. 7 (see also Table II) most CP's are found to be at nearly the same energy position, regardless of polarization. For the sake of completeness, we have derived the selection rules corresponding to the most important optical transitions for the assignment of the characteristic energies, such as those given in Fig. 7. In order to do this we have used the pseudopotential band structure calculated by Grandke and Ley<sup>22</sup> and neglected the spin-orbit interaction (the spin-orbit splitting due to Ge should be  $\sim 0.3$  eV, that due to S  $\sim 0.1$  eV). In Fig. 8 we can see the band structure of GeS, reproduced from Ref. 22 for several directions of the Brillouin zone (BZ), and the possible transitions that are allowed for all three polarizations, corresponding to the  $E_1$ ,  $E_2$ ,  $E_5$ , and  $E_6$  structures. Most of these assignments agree with those given by

Lukeš *et al.*<sup>14</sup> In Fig. 8 dotted arrows represent the allowed transitions for  $\mathbf{E}||\mathbf{a}$ , dashed arrows those for  $\mathbf{E}||\mathbf{b}$  and solid arrows those for  $\mathbf{E}||\mathbf{c}$ . In this figure we can also see that transitions for  $\mathbf{E}||\mathbf{a}$  and  $\mathbf{E}||\mathbf{c}$  corresponding to the observed  $E_1$  structures are allowed for a large number of lines in the BZ with  $A_{1,2} \rightarrow A_{1,2}$  possibly being the strongest for  $\mathbf{E}||\mathbf{c}$ . Thus, we expect  $E_1$  structure to be rather strong for  $\mathbf{E}||\mathbf{a}$  and  $\mathbf{E}||\mathbf{c}$ , in agreement with Fig. 7. The fundamental absorption edge was identified as being direct allowed for  $\mathbf{E}||\mathbf{a}$  and  $\mathbf{E}||\mathbf{c}$  polarizations and direct forbidden for  $\mathbf{E}||\mathbf{b}$ .<sup>18,20</sup> These structures have been attributed to the  $\Lambda_1 \rightarrow \Lambda_1$  transitions.<sup>14,22</sup> In Table II the CP energies obtained in the present work for the three polarizations are listed, together with corresponding values found in the literature. There is good agreement between our data and those of Ref. 14, for  $\mathbf{E}||\mathbf{a}$  and  $\mathbf{E}||\mathbf{b}$ , but it is impossible to analyze weak structures which appeared in previous work and which are also predicted by theory, especially the structures for  $\mathbf{E}||\mathbf{b}$  at 2.52 and 2.63 eV, with only 100-meV energy separation, and those at 2.98 and 3.28 eV (the CP energy 3.096 eV given by us is close to the mean value). Some weak structures between the high-energy wing of the  $E_1$  and  $E_2$  structures for all three polarizations are also seen in Fig. 7, but all of these are masked by the overlap with the strong  $E_1$  and  $E_2$  structures. Finally, in the high-energy region (at  $\sim 4.95$  eV) a relatively noisy weak structure is seen for  $\mathbf{E}||\mathbf{b}$ , in agreement with other experimental and theoretical determinations (see Table II). However, we have not been able to analyze it. Measurements at low temperature should help to verify the existence of these weak structures. The energies of the  $E_1$ ,  $E_2$ ,  $E_3$ , and  $E_6$  structures for  $\mathbf{E}||\mathbf{c}$  (Table II) are in satisfactory agreement with corresponding values from reflectivity spectra.<sup>13</sup>

In Table III the broadening parameters, strengths, phase angles, and the CP type as obtained from our analysis are presented together with the CP type suggested in Ref. 14. The broadening parameters for all three polarizations are, in most cases, large compared with the broadening parameters of diamond and zinc-blende semiconductors.<sup>41,58</sup> This fact emphasizes the possible overlap of separate but closely located structures in GeS and the poor localization of critical points due to the low symmetry of the material. The strengths for the  $E_1$  and  $E_2$  structures are seen to switch strengths for  $\mathbf{E}||\mathbf{a}$  and  $\mathbf{E}||\mathbf{b}$ . For  $\mathbf{E}||\mathbf{a}$  the strongest structures are  $E_3$ ,  $E_5$ , and  $E_6$ , while for  $\mathbf{E}||\mathbf{b}$ ,  $E_3$  and  $E_4$  are strongest. In the case of  $\mathbf{E}||\mathbf{c}$  polarization the strengths are largest in the  $E_1$  and  $E_6$  structures, a fact that is in agreement with the mentioned selection rules. The average strengths for the three polarizations obtained from Table III are  $\bar{E}_a = 3.65(50)$ ,  $\bar{E}_b = 3.5(4)$ , and  $\bar{E}_c = 3.0(4)$  eV.

The oscillator energy  $E_0$  and the interband strength parameter  $E_d$  of Wemple and Di Domenico's model<sup>59</sup> for the electronic dielectric constant, are given by the relations

$$E_0^2 = M_{-1}/M_{-3}, \quad (12a)$$

$$E_d^2 = M_{-1}^3/M_{-3}, \quad (12b)$$

where the  $M_r$ 's correspond to the  $r$ th moments of  $[\epsilon_2(\omega)]_j$  spectra:

$$M_r = \frac{2}{\pi} \int_0^\infty \omega^r \epsilon_2(\omega) d\omega. \quad (13)$$

Since the  $\epsilon_2(\omega)$  spectra contribute to Eqs. (11a) and (11b) mainly in the region of our measurements it is of interest to evaluate these equations with our data. The  $E_0$  ( $E_d$ ) parameters with our upper cutoff  $\omega_M = 5.5$  eV are 3.2 (27), 3.24 (29.5), and 2.79 (19.3) eV for each of the three polarizations, respectively. The  $E_0$  values are in agreement with our crude estimate of the  $\bar{E}_j$  ( $j = a, b, c$ ) energies. These parameters, different for each polarization, are close to those for  $\mathbf{E}||\mathbf{a}$  and  $\mathbf{E}||\mathbf{b}$  given in Ref. 12, as obtained by the best fit to the dispersion of the refractive index.<sup>59</sup> Deviations are probably due to the low cutoff in our spectra. The  $\epsilon_1(\omega=0)$  static dielectric constants for  $\mathbf{E}||\mathbf{a}$  and  $\mathbf{E}||\mathbf{b}$ , as calculated in Ref. 12, are 11.09 and 12.21, respectively. With the assumption that the correction for the  $E_0, E_d$  parameters in the  $\mathbf{E}||\mathbf{c}$  polarization is of the same order we get  $(\epsilon_1)_c(\omega=0) \simeq 8.4$ .

In Fig. 9 we can see the dielectric constant of an assumed overlayer (dashed lines) as calculated with the MAI method with the additional assumption that this overlayer, present only on the cut and polished  $bc$  surface, is uniform and isotropic. Its effective thickness is found to be  $50 \pm 5$  Å from the MAI fit. These data were obtained from measurements in two orientations ( $ca, ba$ ) on the polished face perpendicular to the cleavage plane. In this way, the minimized function  $G(A)$  Eq. (8) depends strongly on the overlayer parameters for both orientations ( $ca, ba$ ). Measurements in each orientation, have been performed for three different angles of incidence. As initial values for the  $\epsilon_a$ ,  $\epsilon_b$ , and  $\epsilon_c$  we have used, for each energy, the values obtained by approximation A. In Fig. 9 we show an attempt to decompose the overlayer into GeS components of all possible orientations plus voids with the EMA approximation Eq. (4). The values of the concentrations  $x$  of the three orientations and of voids for 95% reliability are  $x_a = 0.10(2)$ ,  $x_b = 0.24(4)$ ,  $x_c = 0.38(6)$ , and  $x_v = 0.28(6)$ . The dielectric function of  $a$ -GeS from Ref. 8 is also plotted in Fig. 9. We have tried to model the spectra of  $a$ -GeS in a similar manner as the overlayer spectra, but this procedure leads to a remarkably large fraction of voids (larger than 40%), which is probably meaningless. The large void fraction is needed to take into account the small real and imaginary parts of  $a$ -GeS,<sup>8</sup> as compared with our spectra of crystalline GeS, and their large shift to higher energy.

## V. CONCLUSIONS

In the present work we have used a MAI method to calculate the dielectric constants for all three polarizations of the layer-type semiconductor GeS by means of spectral ellipsometry. Measurements have been carried out on the easy-cleavage planes and a polished surface perpendicular to them. No significant differences are found between this method and an approximate procedure suggested by Aspnes, provided we used large angles of incidence. An overlayer lying on the cut and polished surface has been taken into account. The type of the CP's, the critical-point energies, and the broadening parameters for  $\mathbf{E}$  in the  $a$ ,  $b$ , and  $c$  directions have been obtained by studying

the line shape of the second derivative spectra of the calculated dielectric functions. Despite the fact that the spectra are quite different for the three principal polarizations, the critical-point analysis yields structures that occur at very nearly the same energies regardless of polarization.

#### ACKNOWLEDGMENTS

We would like to express our thanks to E. Schönherr for the crystal growth, G. Kisela and his group at the Max-Planck-Institut (MPI) for the sample preparation and orientation, and H. Bleder and H. Birkner for their help in the construction of the ellipsometer.

\*On leave from First Laboratory of Physics, Aristotle University of Thessaloniki, Thessaloniki, Greece.

- <sup>1</sup>R. Eymard and A. Otto, *Phys. Rev. B* **16**, 1616 (1977).
- <sup>2</sup>R. B. Shaloy, G. B. Fisher, and P. J. Stiles, *Phys. Rev. B* **15**, 2021 (1977).
- <sup>3</sup>H. R. Chandrasekhar, R. G. Humphreys, U. Zwick, and M. Cardona, *Phys. Rev. B* **15**, 2177 (1976).
- <sup>4</sup>R. Car, G. Giucci, and L. Quartapelle, *Phys. Status Solidi B* **86**, 471 (1978).
- <sup>5</sup>G. Valiukonis, F. M. Gashimzade, D. A. Guseinova, G. Krivaite, A. M. Kulibekov, G. S. Orudzhev, and A. Sileika, *Phys. Status Solidi B* **117**, 81 (1983).
- <sup>6</sup>G. Valiukonis, F. M. Gashimzade, D. A. Guseinova, G. Krivaite, M. M. Mamedov, and A. Sileika, *Phys. Status Solidi B* **122**, 623 (1984).
- <sup>7</sup>L. Stourac, M. Zavetova, and A. Abraham, in *Proceedings of the Twelfth International Conference on the Physics of Semiconductors, Stuttgart, 1974*, edited by M. H. Pilkuhn (Tuebner, Stuttgart, 1974), p. 1012.
- <sup>8</sup>L. Pajasova, P. Pajas, O. A. Makarov, and V. M. Zakharov, *Phys. Status Solidi B* **121**, 293 (1984).
- <sup>9</sup>J. D. Wiley, W. J. Buckel, and R. L. Schmidt, *Phys. Rev. B* **13**, 2489 (1976).
- <sup>10</sup>V. Chab and I. Bartos, *Phys. Status Solidi B* **121**, 301 (1984).
- <sup>11</sup>I. Gregora and W. Stetter, *Phys. Status Solidi B* **71**, K187 (1975).
- <sup>12</sup>I. Gregora, B. Velický, and M. Zavetova, *J. Phys. Chem. Solids* **37**, 785 (1976).
- <sup>13</sup>J. D. Wiley, W. J. Buckel, W. Brown, G. W. Fehrenbach, F. J. Himpfel, and E. E. Koch, *Phys. Rev. B* **14**, 697 (1976).
- <sup>14</sup>F. Lukeš, E. Schmidt, J. Humlíček, and P. Dub, *Phys. Status Solidi B* **122**, 675 (1984).
- <sup>15</sup>H. Venghaus and V. Büchner, *Phys. Status Solidi B* **72**, 603 (1975).
- <sup>16</sup>K. F. LIDER and L. E. Solov'ev, *Fiz. Tverd. Tela (Leningrad)* **4**, 1500 (1982) [*Sov. Phys.—Solid State* **4**, 1102 (1962)].
- <sup>17</sup>J. D. Wiley, A. Breitschwerdt, and E. Schönherr, *Solid State Commun.* **17**, 355 (1975).
- <sup>18</sup>J. D. Wiley and D. Thomas, *J. Phys. Chem. Solids* **41**, 801 (1979).
- <sup>19</sup>J. H. Haritonidis, A. P. Lambros, and N. A. Economou, *J. Phys. Chem. Solids* **41**, 659 (1979).
- <sup>20</sup>J. D. Wiley, S. Pennington, and E. Schönherr, *Phys. Status Solidi B* **96**, K37 (1979); **96**, K43 (1979).
- <sup>21</sup>F. Lukeš, E. Schmidt, and A. Lancina, *Solid State Commun.* **39**, 921 (1981).
- <sup>22</sup>T. Grandke and L. Ley, *Phys. Rev. B* **16**, 832 (1977).
- <sup>23</sup>F. Hulliger, in *Structural Chemistry of Layer-Type Phases*, edited by F. Levy (Reidel, Dordrecht, 1976), Vol. 5, Chap. 3.
- <sup>24</sup>J. C. Phillips, *Bonds and Bands in Semiconductors* (Academic, New York, 1973).
- <sup>25</sup>W. H. Zachariasen, *Phys. Rev.* **40**, 917 (1932). G. Bissert and K. F. Hesse, *Acta Crystallogr. Sect. B* **34**, 1322 (1978).
- <sup>26</sup>D. E. Aspnes, *J. Opt. Soc. Am.* **70**, 1275 (1980).
- <sup>27</sup>S. Teitler and B. Hervis, *J. Opt. Soc. Am.* **60**, 830 (1970).
- <sup>28</sup>D. W. Berreman and T. J. Scheffer, *Phys. Rev. Lett.* **25**, 577 (1970).
- <sup>29</sup>D. W. Berreman, *J. Opt. Soc. Am.* **62**, 502 (1972).
- <sup>30</sup>D. J. De Smet, *Surf. Sci.* **56**, 293 (1976).
- <sup>31</sup>R. M. A. Azzam and N. M. Bashara, *Ellipsometry and Polarized Light* (North-Holland, Amsterdam, 1977), Chap. 4.
- <sup>32</sup>R. T. Jacobsen, *J. Opt. Soc. Am.* **54**, 1170 (1964).
- <sup>33</sup>D. A. G. Bruggeman, *Ann. Phys. (Leipzig)* **24**, 636 (1935).
- <sup>34</sup>D. E. Aspnes, *Thin Solid Films* **89**, 249 (1982).
- <sup>35</sup>R. T. Jacobsen and M. Kerker, *J. Opt. Soc. Am.* **57**, 751 (1967).
- <sup>36</sup>S. Logothetidis, S. Ves, and J. Spyridelis, *Phys. Status Solidi B* **122**, 613 (1984).
- <sup>37</sup>F. Meyer, E. E. De Kluizenaar, and D. Den Engelsens, *J. Opt. Soc. Am.* **63**, 529 (1973).
- <sup>38</sup>E. Schönherr and W. Stetter, *J. Cryst. Growth* **30**, 96 (1975).
- <sup>39</sup>D. E. Aspnes, *Appl. Phys. Lett.* **39**, 316 (1981).
- <sup>40</sup>D. E. Aspnes and A. A. Studna, *Appl. Opt.* **14**, 220 (1975).
- <sup>41</sup>L. Viña, S. Logothetidis, and M. Cardona, *Phys. Rev. B* **30**, 1979 (1984).
- <sup>42</sup>D. E. Aspnes, J. C. Phillips, K. L. Tai, and P. M. Bridenbaugh, *Phys. Rev. B* **23**, 816 (1981).
- <sup>43</sup>H. R. Phillip and H. Ehrenreich, *Phys. Rev.* **129**, 1558 (1963); P. Nozieres and D. Pines, *ibid.* **113**, 1254 (1959).
- <sup>44</sup>M. Cardona, *J. Appl. Phys.* **36**, 2181 (1965).
- <sup>45</sup>H. Asahina and A. Morita, *J. Phys. C* **17**, 1839 (1984).
- <sup>46</sup>L. Viña and M. Cardona, *Phys. Rev. B* **29**, 6739 (1984); D. E. Aspnes, *Physica (Utrecht)* **117-118B**, 359 (1983).
- <sup>47</sup>P. Soukiassian, J. Cazaux, and J. Perrin, *Phys. Status Solidi B* **66**, 151 (1974).
- <sup>48</sup>Y. Toyozawa, M. Inoue, T. Inui, M. Okazaki, and E. Hanamura, *J. Phys. Soc. Jpn. Suppl.* **21**, 133 (1967); *J. Phys. Soc. Jpn.* **22**, 1337 (1967).
- <sup>49</sup>M. Cardona, *Modulation Spectroscopy*, Suppl. 11 of *Solid State Physics*, edited by F. Seitz, D. Turnbull, and H. Ehrenreich (Academic, New York, 1969).
- <sup>50</sup>J. E. Rowe and D. E. Aspnes, *Phys. Rev. Lett.* **25**, 162 (1970).
- <sup>51</sup>F. Bassani and G. Pastori Parravicini, in *Electronic States and Optical Transitions in Solids*, edited by R. A. Ballinger (Pergamon, Oxford, 1975).
- <sup>52</sup>Y. Takao, H. Asahina, and A. Morita, *J. Phys. Soc. Jpn.* **50**, 3362 (1981).
- <sup>53</sup>H. Asahina, K. Shindo, and A. Morita, *J. Phys. Soc. Jpn.* **51**, 1193 (1982).
- <sup>54</sup>X. Polatoglou, Ph.D. thesis, University of Thessaloniki, Greece, 1984.
- <sup>55</sup>M. Cardona and D. L. Greenaway, *Phys. Rev.* **133**, A1685 (1964).
- <sup>56</sup>G. Lucovsky, R. M. Martin, and E. Burstein, in *Proceedings of the Conference on the Physics of IV-VI Compounds and Alloys*, edited by S. Rabi (Gordon and Breach, London, 1973).
- <sup>57</sup>H. Kawamura, *Comments Solid State Phys.* **9**, 55 (1979).
- <sup>58</sup>S. Logothetidis, L. Viña, and M. Cardona, *Phys. Rev. B* (to be published); L. Viña, H. Höchst, and M. Cardona, *Phys. Rev. B* **31**, 958 (1985).
- <sup>59</sup>S. H. Wemple and M. Di Domenico, Jr., *Phys. Rev. B* **3**, 1338 (1971); *Phys. Rev. Lett.* **23**, 1156 (1969).